HHS Public Access

Author manuscript

ACS Chem Neurosci. Author manuscript; available in PMC 2016 May 25.

Published in final edited form as:

ACS Chem Neurosci. 2015 April 15; 6(4): 535–541. doi:10.1021/acschemneuro.5b00055.

PET neuroimaging studies of [^{18}F]CABS13 in a double transgenic mouse model of Alzheimer's disease and non-human primates

Steven H. Liang[1,2], **Jason P. Holland**[2], **Nickeisha A. Stephenson**[1,2], **Alina Kassenbrock**[1], **Benjamin H. Rotstein**[1,2], **Cory P. Daignault**[1], **Rebecca Lewis**[1], **Lee Collier**[1,2,3], **Jacob M. Hooker**[2,4], and **Neil Vasdev**[1,2,*]

[1]Division of Nuclear Medicine and Molecular Imaging & Center for Advanced Medical Imaging Sciences, Massachusetts General Hospital, Boston, Massachusetts, USA

[2]Department of Radiology, Harvard Medical School, Boston, Massachusetts

[3]Advion, Inc., Ithaca, New York, USA

[4]Athinoula A. Martinos Center for Biomedical Imaging, Massachusetts General Hospital, Charlestown, Massachusetts, USA

Abstract

Fluorine-18 labeled 2-fluoro-8-hydroxyquinoline ([^{18}F]CABS13) is a promising positron emission tomography (PET) radiopharmaceutical based on a metal chelator developed to probe the "metal hypothesis of Alzheimer's disease". Herein, a practical radiosynthesis of [^{18}F]CABS13 was achieved by radiofluorination followed by deprotection of an *O*-benzyloxymethyl group. Automated production and formulation of [^{18}F]CABS13 resulted in 19 ± 5% uncorrected radiochemical yield, relative to starting [^{18}F]fluoride, with ≥95% chemical and radiochemical purities, and high specific activity (>2.5 Ci/μmol) within 80 minutes. Temporal PET neuroimaging studies were carried out in female transgenic B6C3- Tg(APPswe,PSEN1dE9)85Dbo/J (APP/PS1) and age-matched wild-type (WT) B6C3F1/J control mice at 3, 7 and 10 months of age. [^{18}F]CABS13 showed an overall higher uptake and retention of radioactivity in the central nervous system of APP/PS1 mice *versus* WT mice with increasing age. However, PET/magnetic resonance imaging in normal non-human primates revealed that the tracer had low uptake in the brain and rapid formation of a hydrophilic radiometabolite. Identification of more metabolically stable ^{18}F-hydroxyquinolines that can be readily accessed by the radiochemical strategy presented herein is underway.

Keywords

[^{18}F]CABS13; metal hypothesis of Alzheimer's disease; rodents; non-human primates; transgenic mice; APP/PS1

*Corresponding author: Tel: 1-617-643-4736, Fax: 1-617-726-6165, ; Email: vasdev.neil@mgh.harvard.edu

Supporting information

Synthesis of precursors, automation of radiosynthesis and microPET imagings of [^{18}F]CABS13 in mice and non human primates are included in the supporting information. This information is available free of charge via the Internet at http://pubs.acs.org/.

INTRODUCTION

Detection of amyloid-beta protein aggregates (Aβ plaques) in brain tissues with positron emission tomography (PET) is an intense area of clinical research for Alzheimer's Disease (AD) and related dementias.[1] Several PET radiopharmaceuticals have been developed to interrogate Aβ plaques, including 2-(4'-[^{11}C]methylaminophenyl)-6-hydroxybenzothiazole (^{11}C-Pittsburgh Compound B; [^{11}C]PiB), 2-(2-[^{18}F]fluoro-6-(methylamino)pyridin-3-yl)benzofuran-5-ol ([^{18}F]NAV4694; [^{18}F]AZD4694), and three tracers recently been approved for use in patients with cognitive impairment by the U.S. Food and Drug Administration: (*E*)-4-(2-(6-(2-(2-(2-([^{18}F]fluoroethoxy)ethoxy)ethoxy)pyridin-3- yl)vinyl)-*N*-methyl benzenamine ([^{18}F]Florbetapir), 2-[3-[^{18}F)fluoro-4-(methylamino)phenyl]-1,3-benzothiazol-6-ol ([^{18}F]Flutametamol) and 4-(*E*)-2-(4-(2-(2-(2-[^{18}F]fluoroethoxy]ethoxy)ethoxy)phenyl)vinyl)-*N*-methylaniline ([^{18}F]Florbetaben).[2] Although clinical trials have been realized with the above-mentioned radiopharmaceuticals, these agents are still under further development to study their sensitivity to low levels of Aβ,[3] as well as to explore the correlation of memory decline in healthy subjects and patients with early mild cognitive impairment.[4] Furthermore, recent failures of numerous anti-amyloid therapies in the final stages of clinical testing have raised questions about the value and purported specificity of Aβ imaging with the existing PET radiopharmaceuticals.[3] New radiotracers for specific Aβ quantification are desperately needed, not only as early detection diagnostics, but also to enable accurate classification of subjects for clinical trials and to assess therapeutic response.[5]

The "metal hypothesis of AD"[6-11] stems from a complex and growing body of evidence showing that various metal ions promote Aβ aggregation from the stage of oligomer formation, in addition to playing critical physiological roles in normal synaptic transmission and neuronal survival. In particular, Aβ has Zn and Cu binding sites and these metal ions are enriched in Aβ aggregates in transgenic AD mice as well as in patients, as attributed to insufficient metal reuptake.[12-14] It is known that Zn, Cu and Fe ions are involved in the Aβ deposition and stabilization, and metal chelating agents can facilitate dissolution of Aβ deposits by preventing metal-Aβ interaction,[15] thereby representing both therapeutic and diagnostic strategies for AD and related dementias.[16-20] Development of a single-photon emission computed tomography (SPECT) or PET radiotracer based on a recognized metal chelator could advance our understanding of neurological disorders that are affected by dysregulation of metal functions, and may prove useful in monitoring therapy for patients with neurodegenerative diseases.

A prototypical hydroxyquinoline-based drug, clioquinol (5-chloro-7-iodo-8-hydroxyquinoline; CQ), prevents Aβ toxicity *in vitro* and out-competes Aβ for metal ions without changing the activity of Zn/Cu- dependent enzymes.[15,21] Further investigations revealed that CQ not only prevents or reverses extracellular Aβ aggregation, but also transports metal ions across cell membranes to increase intracellular metal concentration, thereby initiating protective cell signaling.[5, 13] These efforts stimulated the development of radiolabeled CQ and its derivatives for molecular imaging studies. An early attempt to use [^{123}I]CQ as an imaging marker via SPECT failed due to low brain uptake in preclinical and clinical research.[22,23] Our laboratory discovered the first PET radiotracer to probe the

metal hypothesis of AD, namely [^{18}F]2-fluoro-8-hydroxyquinoline ([^{18}F]CABS13), and carried out a promising preliminary PET imaging study in a transgenic mouse model of AD in aged rodents with well- developed plaque formation (10-12 months).[24] It is noteworthy that exploration of the "metal hypothesis of AD" with PET is actively pursued by several laboratories, with recent accounts of carbon-11 and fluorine-18 labeled analogs of L2-b (*N*^{1},*N*^{1}-dimethyl-*N*^{4}-(pyridin-2-ylmethyl)benzene-1,4-diamine)s[25] and copper-64-labeled bis(thiosemicarbazonato)Cu^{II}complexes.[26,27]

While our preliminary studies showed that [^{18}F]CABS13 may be promising for imaging Aβ plaques in vivo, the lack of a facile and automated radiosynthesis for this tracer and related hydroxyquinolines has hindered further development. **Scheme 1A** shows our original synthesis of [^{18}F]CABS13 which employed a palladium-catalyzed hydrogenation for mild deprotection of an *O*-benzyl protecting group following radiofluorination (manual synthesis), [24] and our recently adapted automated process using a flow radiofluorination and flow hydrogenation devices (microfluidic hydrogenation).[28] Herein we describe a novel radiosynthetic strategy for the facile preparation of [^{18}F]CABS13, longitudinal PET-CT imaging studies in a double transgenic mouse model of AD spanning from early to mature plaque stages, and PET/magnetic resonance (MR) imaging in healthy *Papio anubis* baboons.

RESULTS AND DISCUSSION

As shown in **Scheme 1A**, a synthesis of [^{18}F]CABS13 was carried out by reaction of [^{18}F]NEt$_4$F with a novel benzyloxy methyl (BOM) protected precursor **1**, followed by a trifluoroacetic acid (TFA) mediated deprotection. The radiosynthesis of [^{18}F]CABS13 was automated using a commercial radiofluorination device (GE Tracerlab FX$_{F-N}$) in an uncorrected radiochemical yield of 19 ± 5%, relative to starting [^{18}F]fluoride, with high chemical and radiochemical purities (both ≥95%) as well as high specific activity (> 2.5 Ci/μmol). The product was formulated in 10% ethanol in saline solution and no radiolysis was detected over 6 hours. Greater than 50% increase of radiochemical yield and more than 2-fold increase in specific activities were achieved compared with our original method to synthesize [^{18}F]CABS13.[24]

The reaction underwent an activation step via coordination to phenolic oxygen, followed by deprotection *in situ* (**Scheme 1B**, route A) at elevated temperature (see supplementary information). When aqueous acids were used, an interfering pathway decomposed the desired ^{18}F-labeled hydroxyquinoline. Specifically, a nucleophile from reaction mixture was found to displace the ^{18}F- fluorine at the 2-position of the pyridine, thereby generating non-radioactive by-products and free fluoride (**Scheme 1B**, route B). Such undesirable side-reactions could become a major hurdle to removing protecting groups in molecules bearing 2-[^{18}F]fluoropyridine moieties, which are widely-used building blocks, and can be problematic towards other functional groups that may undergo acid-catalyzed nucleophilic displacement reactions. Notably, the di-t-butyloxycarbonyl (Boc) protected precursor was not stable under basic labeling conditions and provided inferior radiochemical conversions, compared to **1**. The utilization of the *O*-BOM group was effective and can be easily removed under anhydrous acidic conditions, thereby obviating the need of either manual synthesis or

specialized device to prepare [^{18}F]CABS13.[24,28] This method also provides an alternative protection/deprotection method for radiotracer design and should prove to be broadly applicable for synthesis of hydroxyquinolines and related scaffolds.

Dynamic PET/CT imaging was carried out to investigate temporal differences in [^{18}F]CABS13 binding in double transgenic (APP/PS1) mice at ages 3, 7 and 10 months along with age-matched wild- type controls (WT; B6C3F1/J) (**Figure 1**). Axial, coronal and sagittal images of the murine brains summed from 5-10 min post-injection of [^{18}F]CABS13 are presented in **Figure 1A**. As predicted, increased uptake and retention of radiotracer binding was observed in the whole brains of transgenic mice compared with WT controls. The time-activity curves revealed a similar trend of increased brain penetration with increasingly higher brain uptake at 3, 7 and 10 months for both groups of mice (**Figure 1B**). Maximum uptake (whole brain peak uptake SUV(mean) = 2.2, 3.2 and 4.6, in transgenic mice and 1.8, 1.4 and 2.9 for WT controls at 3,7 and 10 months, respectively) was observed in both genotypes after one minute post-injection of the radiotracer, followed by a relatively slow washout in the transgenic mice and a more rapid washout in WT mice as the radioactivity cleared from normal tissues. A comparison of the area under the curve (AUC) analysis (**Figure 1C**) over time for the respected genotypes, underscores the trends observed in the TACs. In addition to our preliminary study on well-developed AD mice (10-12 months),[24] the temporal PET/CT imaging studies from early to well-developed stages (3-10 months) with [^{18}F]CABS13 in transgenic mouse models of AD presented herein provides further and consistent evidence for a PET tracer with potential to probe the “metal hypothesis of AD”.

Encouraged by the temporal PET imaging of [^{18}F]CABS13 in rodent models, we carried out preliminary PET/MR imaging studies in normal baboons. Analysis of the PET/MR imaging data reveals that radioactivity enters the cranium and is observed in the torcula reaching a maximum at approximately five minutes post injection of the radiotracer (**Figure 2**). Over time ($t_{1/2}$ ~ 5 min) the radioactivity distributes to the superior sagittal, occipital and transverse sinuses. A very small proportion of the radioactivity at these early time points appears in the brain; however, it is difficult to determine if the activity observed represents the blood pool uptake within the brain. A second imaging study was carried out with arterial plasma analysis, and was consistent with the previous scan. The time-activity curve of radioactivity in the plasma is well matched to that derived from a region of interest placed in the torcula as would be expected. Further analysis of the radioactivity in arterial plasma suggests that the majority (>90%) of circulating radioactivity at 5 minutes post administration of the radiotracer is a polar radiometabolite which is unlikely free [^{18}F]fluoride because of the absence of noted uptake in bone regions. Although specific binding and metabolism (potentially attributed to sulfation and/or glucuronidation) may be different in higher species, given the fast metabolism and low retention of [^{18}F]CABS13 in the non-human primate brain, this ^{18}F-labeled hydroxyquinoline was not further evaluated.

In summary, we demonstrated a novel high-yielding radiosynthetic method to prepare [^{18}F]CABS13 employing benzyloxymethyl as a handle for protection and deprotection of a phenolic functionality under metal-free anhydrous conditions. Despite the increased radiotracer retention in the brains of APP/PS1 mice over time, rapid metabolism and low

brain penetration observed in the non-human primate imaging studies will preclude its further use. The radiosynthetic strategy developed herein represents the effective use of a BOM protecting group to eliminate the need for hazardous transition-metal mediated hydrogenations in radiochemistry, enabled facile automation, and should be broadly applicable for the synthesis of radiolabeled hydroxyquinolines and related scaffolds. Our current efforts will take advantage of protection/deprotection strategy and will be directed towards radiolabeling either at the non-activated aromatic phenolic moiety via our recently described hypervalent iodonium ylide method for radiofluorination of electron-rich aromatic rings,[29] or at the aliphatic alkyl chain based on 5,7-dichloro- 2-(dimethylamino)methyl-8-quinolinol (PBT2),[30] a newer generation hydroxyquinoline based metal chelator in phase II clinical trials.

METHODS

Synthesis of [^{18}F]CABS13

Detailed procedures of precursor synthesis are provided in the supplementary information. The radiofluorination was carried out between precursor **1** (6 mg in 1.1 mL DMF) and [^{18}F]Et_4NF (prepared with tetraethylammonium bicarbonate (14mg) and aqueous [^{18}F]fluoride, co-evaporated with CH_3CN three times) at 140°C for 15 min to yield ^{18}F-labeled compound **2**. The deprotection reactions were tested in various acidic conditions at different temperatures in order to identify the optimal conditions for the synthesis of [^{18}F]CABS13. Radiochemical conversion yields were determined by radio-TLC and the identity of the molecule was confirmed by radio-HPLC. The optimized reaction parameters were selected for automated synthesis of [^{18}F]CABS13. Detailed procedures are provided in the supplementary information. Analyses of radioactive mixtures were performed by HPLC with an in-line UV (λ = 254 nm) detector in series with a CsI pin diode radioactivity detector. To determine the identity of [^{18}F]CABS13, aliquots of the formulated product were injected onto an analytical HPLC system using an analytical Luna C-18 column (150 × 4.6 mm, 5 μm) and eluted with mobile phase (CH_3CN / 0.1N ammonium formate, 70:30 v/v) with a flow rate of 1 mL/min, monitored at λ = 254 nm. The major radiochemical product was identified as [^{18}F]CABS13 (t_R = ~5.8 min). A mass calibration curve (λ = 254 nm) was generated from known concentrations of CABS13 in solutions to determine the specific activity.

PET imaging studies in APP/PS1 and wild-type control mice

All animal experiments were conducted in compliance with Institutional Animal Care and Use Committee (IACUC) guidelines and the *Guide for the Care and Use of Laboratory Animals*. Female, wild-type B6C3F1/J mice (6 – 8 weeks old) and transgenic B6C3-Tg(APPswe,PSEN1dE9)85Dbo/J (APP/PS1; Stock No.: 034829-JAX or MMRRC No. 034) mice were obtained from Jackson Laboratory (Bar Harbor, ME). Mice were provided with food and water *ad libitum* and were allowed to acclimatize for 1 month prior to conducting PET/CT and biodistribution experiments. Dynamic PET/CT imaging experiments were conducted on a dedicated small-animal PET/CT scanner (eXplore Vista-CT, Sedecal, Algete, Spain) equipped with VISTA-CT version 4.11 software. In separate studies (n=3), mice were administered formulations of [^{18}F]CABS13 (~4.0 – 16.0 MBq [~100 – 432 μCi], specific

activity of > 2 Ci/μmol, in 200 μL sterile PBS, pH7.4, ≤5% v/v EtOH) *via* intravenous (i.v.) tail-vein injection using a catheter. Approximately 5 minutes prior to recording PET images, mice were anesthetized by inhalation of 3–4% isoflurane (Baxter Healthcare, Deerfield, IL)/ oxygen gas mixture and, a catheter was inserted into the tail-vein, and then mice were transferred to the scanner bed and placed in the prone position. Anesthesia was maintained with 1-2% isoflurane/oxygen gas mixture (flow rate ~5 L/min). Co-registered dynamic PET/CT images were recorded for a total of 20 – 30 min post-injection radiotracer injection ($n \geq 3$ mice/time point). List-mode data were acquired for 20 – 30 min per scan using a γ-ray energy window of 250–700 keV. To ensure that the activity bolus was measured, PET/CT data acquisition was initiated 20 s prior to injecting the radioactivity. Data were processed by 3-dimensional Fourier re-binning (3D-FORE), and images were reconstructed using 2-demensional ordered-subset expectation maximum (2D-OSEM) algorithm. Image data were normalized to correct for non-uniformity of response of the PET, dead-time count losses, positron branching ratio, and physical decay to the time of injection, but no attenuation, scatter, or partial- volume averaging correction was applied. An empirically determined system calibration factor (in units of Bq/cps) combined with the decay corrected administered activity and the animal weight were used to parameterize image activity in terms of the standardized uptake value (SUV). Manually drawn 2- dimensional regions-of-interest (ROIs) or 3-dimensional volumes-of-interest (VOIs) were used to determine the maximum and mean SUV radiotracer uptake in various tissues. Time-activity curves (TACs) were generated from ROI analysis on dynamic PET/CT data using 20 s frames. CT images were recorded using an X-ray current of 300 μA, 360 projections, and an image size of 63.8 mm × 63.8 mm × 46.0 mm. Data were acquired using the Vista CT 4.11 Build 701 software, and reconstructed images were analyzed by using VivoQuant® 1.23 (InviCRO, LLC, Boston, MA). Data and statistical analyses were performed using GraphPad Prism 5.01 (GraphPad Software, Inc., La Jolla, CA) and Microsoft Excel.

PET imaging studies in nonhuman primates

One adult baboon (Papio Anubis, female, 5 y.o., 14.1 kg), deprived of food for 12 h prior to imaging experiments, was included in the study (n = 2). Intramuscular ketamine (10 mg/kg) was administered for animal preparation and intubation. The animal was catheterized antecubitally for hydration and radiotracer injection. In one experiment, a radial arterial line was placed for plasma and metabolite analysis. For maintenance of anesthesia throughout the imaging study, the baboon was provided 1 – 1.5% isoflurane (Forane) in a mixture of medical oxygen and nitrogen. Body temperature was maintained by heated water blanket. Vital signs including end tidal CO_2, SpO_2, heart rate, respiration rate and blood pressure were monitored and maintained within normal ranges during the studies. PET and MRI images were acquired on a 3T Siemens TIM-Trio with a BrainPET insert (Siemens, Erlangen, Germany). A custom PET/MRI compatible 8-channel array coil for non- human primate brain imaging was used to improve image signal and quality. Dynamic PET image acquisition was initiated concurrently with the administration of the radiotracer (5 ± 0.2 mCi, 2 scans) in a homogenous solution of 10% ethanol and 90% isotonic saline, and continued for duration of 120 min. A high-resolution anatomical scan using multi-echo MPRAGE sequence (TR = 2530 ms, TE1/TE2/TE3/TE4 = 1.64/3.5/5.36/7.22 ms, TI = 1200 ms, flip angle = 7°, and 1 mm isotropic) was acquired for anatomic coregistration. Blood

sampling from the radial arterial line occurred nominally every 10 seconds for the first 3 minutes (~1 mL each) after radiotracer administration, followed by sampling at 5, 10, 20, 30, 45, 60, and 90 minute time points (~3 mL each) for plasma and metabolite analysis. Arterial samples were centrifuged to obtain plasma, which was then removed and placed in an automated gamma counter that was calibrated with the PET scanner and using a 350 – 600 keV window. Beginning with the arterial sample acquired at 5 minutes after radiotracer administration, an aliquot (300 μL) of plasma was added to acetonitrile (300 μL) and centrifuged for 1 – 2 minutes to obtain protein-free plasma (PFP). An aliquot (300 μL) of PFP was diluted with deionized water (2 mL), and loaded onto a customized automated robot, fitted with Phenomenex Strata-X 500 mg SPE cartridges that were primed with ethanol (2 mL) and deionized water (20 mL). Solutions of PFP were loaded on SPE cartridges, and then extracted sequentially with 4 mL of 100% 0.1 N ammonium formation (AMF); 10% CH_3CN/0.1N AMF; 20% CH_3CN/0.1N AMF; 30% CH_3CN/0.1N AMF; 40% CH_3CN/0.1N AMF; 70% CH_3CN/0.1N AMF; 100% CH_3CN. This program had been previously tested with [^{18}F]CABS13 to determine its retention properties. Each eluent sample was counted in an automated gamma counter to determine the presence of radiolabeled metabolites.

Supplementary Material

Refer to Web version on PubMed Central for supplementary material.

References

1. Zhu L, Ploessl K, Kung HF. PET/SPECT imaging agents for neurodegenerative diseases. Chem. Soc. Rev. 2014; 43:6683–6691. [PubMed: 24676152]
2. McConathy J, Sheline YI. Imaging Biomarkers Associated With Cognitive Decline: A Review. Biol. Psychiatry.
3. Kepe V, Moghbel MC, Langstrom B, Zaidi H, Vinters HV, Huang S-C, Satyamurthy N, Doudet D, Mishani E, Cohen RM, Hoilund-Carlsen PF, Alavi A, Barrio JR. Amyloid-β Positron Emission Tomography Imaging Probes: A Critical Review. J. Alzheimers Dis. 2013; 36:613–631. [PubMed: 23648516]
4. Villemagne VL, Burnham S, Bourgeat P, Brown B, Ellis KA, Salvado O, Szoeke C, Macaulay SL, Martins R, Maruff P, Ames D, Rowe CC, Masters CL. Amyloid β deposition, neurodegeneration, and cognitive decline in sporadic Alzheimer's disease: a prospective cohort study. The Lancet Neurology. 2013; 12:357–367. [PubMed: 23477989]
5. Holland JP, Liang SH, Rotstein BH, Collier TL, Stephenson NA, Greguric I, Vasdev N. Alternative approaches for PET radiotracer development in Alzheimer's disease: imaging beyond plaque. J. Labelled. Compd. Radiopharm. 2014; 57:323–331.
6. Crouch PJ, Barnham KJ. Therapeutic Redistribution of Metal Ions To Treat Alzheimer's Disease. Acc. Chem. Res. 2012; 45:1604–1611. [PubMed: 22747493]
7. Frederickson CJ, Koh J-Y, Bush AI. The neurobiology of zinc in health and disease. Nat. Rev. Neurosci. 2005; 6:449–462. [PubMed: 15891778]
8. Watt NT, Whitehouse IJ, Hooper NM. The Role of Zinc in Alzheimer's Disease. Int. J. Alzheimers Dis. 2011:971021. Article ID.
9. Bush AI. Drug Development Based on the Metals Hypothesis of Alzheimer's Disease. J. Alzheimers Dis. 2008; 15:223–240. [PubMed: 18953111]
10. Bush AI, Tanzi RE. Therapeutics for Alzheimer's Disease Based on the Metal Hypothesis. Neurotherapeutics. 2008; 5:421–432. [PubMed: 18625454]

11. Savelieff MG, Lee S, Liu Y, Lim MH. Untangling Amyloid-β, Tau, and Metals in Alzheimer's Disease. ACS Chem. Biol. 2013; 8:856–865. [PubMed: 23506614]
12. Lee J-Y, Mook-Jung I, Koh J-Y. Histochemically Reactive Zinc in Plaques of the Swedish Mutant β-Amyloid Precursor Protein Transgenic Mice. J. Neurosci. 1999; 19:RC10. [PubMed: 10341271]
13. Lovell MA, Robertson JD, Teesdale WJ, Campbell JL, Markesbery WR. Copper, iron and zinc in Alzheimer's disease senile plaques. J. Neurol. Sci. 1998; 158:47–52. [PubMed: 9667777]
14. Suh SW, Jensen KB, Jensen MS, Silva DS, Kesslak PJ, Danscher G, Frederickson CJ. Histochemically-reactive zinc in amyloid plaques, angiopathy, and degenerating neurons of Alzheimer's diseased brains. Brain Res. 2000; 852:274–278. [PubMed: 10678753]
15. Cherny RA, Atwood CS, Xilinas ME, Gray DN, Jones WD, McLean CA, Barnham KJ, Volitakis I, Fraser FW, Kim Y-S, Huang X, Goldstein LE, Moir RD, Lim JT, Beyreuther K, Zheng H, Tanzi RE, Masters CL, Bush AI. Treatment with a Copper-Zinc Chelator Markedly and Rapidly Inhibits Aβ-Amyloid Accumulation in Alzheimer's Disease Transgenic Mice. Neuron. 2001; 30:665–676. [PubMed: 11430801]
16. Cherny RA, Atwood CS, Xilinas ME, Gray DN, Jones WD, McLean CA, Barnham KJ, Volitakis I, Fraser FW, Kim Y-S, Huang X, Goldstein LE, Moir RD, Lim JT, Beyreuther K, Zheng H, Tanzi RE, Masters CL, Bush AI. Treatment with a copper-zinc chelator markedly and rapidly inhibits ß-amyloid accumulation in Alzheimer's disease transgenic mice. Neuron. 2001; 30:665–676. [PubMed: 11430801]
17. Lee JY, Friedman JE, Angel I, Kozak A, Koh JY. The lipophilic metal chelator DP-109 reduces amyloid pathology in brains of human beta-amyloid precursor protein transgenic mice. Neurobiol Aging. 2004; 25:1315–1321. [PubMed: 15465629]
18. Adlard PA, Cherny RA, Finkelstein DI, Gautier E, Robb E, Cortes M, Volitakis I, Liu X, Smith JP, Perez K, Laughton K, Li QX, Charman SA, Nicolazzo JA, Wilkins S, Deleva K, Lynch T, Kok G, Ritchie CW, Tanzi RE, Cappai R, Masters CL, Barnham KJ, Bush AI. Rapid restoration of cognition in Alzheimer's transgenic mice with 8-hydroxy quinoline analogs is associated with decreased interstitial Abeta. Neuron. 2008; 59:43–55. [PubMed: 18614028]
19. Lannfelt L, Blennow K, Zetterberg H, Batsman S, Ames D, Harrison J, Masters CL, Targum S, Bush AI, Murdoch R, Wilson J, Ritchie CW. Safety, efficacy, and biomarker findings of PBT2 in targeting Abeta as a modifying therapy for Alzheimer's disease: a phase IIa, double-blind, randomised, placebo-controlled trial. Lancet neurology. 2008; 7:779–786. [PubMed: 18672400]
20. Faux NG, Ritchie CW, Gunn A, Rembach A, Tsatsanis A, Bedo J, Harrison J, Lannfelt L, Blennow K, Zetterberg H, Ingelsson M, Masters CL, Tanzi RE, Cummings JL, Herd CM, Bush AI. PBT2 rapidly improves cognition in Alzheimer's Disease: additional phase II analyses. J Alzheimers Dis. 2010; 20:509–516. [PubMed: 20164561]
21. Bareggi SR, Cornelli U. Clioquinol: Review of its Mechanisms of Action and Clinical Uses in Neurodegenerative Disorders. CNS Neurosci. Ther. 2012; 18:41–46. [PubMed: 21199452]
22. Papazian V, Jackson T, Pham T, Liu X, Greguric I, Loc'h C, Rowe C, Villemagne V, Masters CL, Katsifis A. The preparation of $^{123/125}$I-clioquinol for the study of Aβ protein in Alzheimer's disease. J. Labelled. Compd. Radiopharm. 2005; 48:473–484.
23. Opazo C, Luza S, Villemagne VL, Volitakis I, Rowe C, Barnham KJ, Strozyk D, Masters CL, Cherny RA, Bush AI. Radioiodinated clioquinol as a biomarker for β-amyloid: Zn^{2+} complexes in Alzheimer's disease. Aging Cell. 2006; 5:69–79. [PubMed: 16441845]
24. Vasdev N, Cao P, van Oosten EM, Wilson AA, Houle S, Hao G, Sun X, Slavine N, Alhasan M, Antich PP, Bonte FJ, Kulkarni P. Synthesis and PET imaging studies of [^{18}F]2-fluoroquinolin-8-ol ([^{18}F]CABS13) in transgenic mouse models of Alzheimer's disease. Med. Chem. Commum. 2012; 3:1228–1230.
25. Cary BP, Brooks AF, Fawaz MV, Shao X, Desmond TJ, Carpenter GM, Sherman P, Quesada CA, Albin RL, Scott PJH. Targeting Metal-Aβ Aggregates with Bifunctional Radioligand [^{11}C]L2-b and a Fluorine-18 Analogue [^{18}F]FL2-b. ACS Med. Chem. Lett. 2014
26. Lim S, Paterson BM, Fodero-Tavoletti MT, O'Keefe GJ, Cappai R, Barnham KJ, Villemagne VL, Donnelly PS. A copper radiopharmaceutical for diagnostic imaging of Alzheimer's disease: a bis(thiosemicarbazonato)copper(ii) complex that binds to amyloid-[small beta] plaques. Chem. Commun. 2010; 46:5437–5439.

27. Hickey JL, Lim S, Hayne DJ, Paterson BM, White JM, Villemagne VL, Roselt P, Binns D, Cullinane C, Jeffery CM, Price RI, Barnham KJ, Donnelly PS. Diagnostic Imaging Agents for Alzheimer's Disease: Copper Radiopharmaceuticals that Target Aβ Plaques. J. Am. Chem . Soc. 2013; 135:16120–16132. [PubMed: 24070589]

28. Liang SH, Collier TL, Rotstein BH, Lewis R, Steck M, Vasdev N. Rapid microfluidic flow hydrogenation for reduction or deprotection of ^{18}F-labeled compounds. Chem. Commun. 2013; 49:8755–8757.

29. Rotstein BH, Stephenson NA, Vasdev N, Liang SH. Spirocyclic hypervalent iodine(III)- mediated radiofluorination of non-activated and hindered aromatics. Nat. Commun. 2014; 5

30. Faux NG, Ritchie CW, Gunn A, Rembach A, Tsatsanis A, Bedo J, Harrison J, Lannfelt L, Blennow K, Zetterberg H, Ingelsson M, Masters CL, Tanzi RE, Cummings JL, Herd CM, Bush AI. PBT2 Rapidly Improves Cognition in Alzheimer's Disease: Additional Phase II Analyses. J. Alzheimers Dis. 2010; 20:509–516. [PubMed: 20164561]

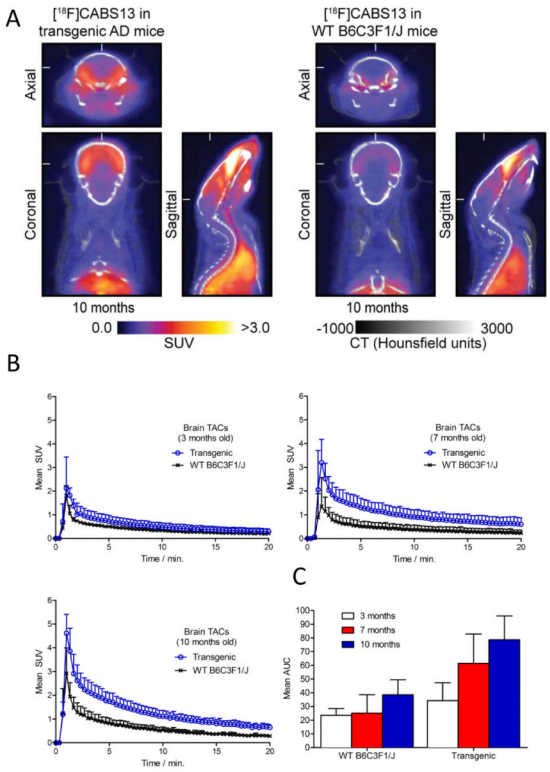

Figure 1.

Longitudinal PET studies in APP/PS1 transgenic mice of AD versus wild-type controls. (A) PET images (axial, coronal and sagittal) summed at 5-10 min post-injection of 10 month-old transgenic mice (left) versus WT controls (right); (B) Time-activity curves and (C) AUC measurement in whole brain between transgenic mice of AD versus WT controls in 3, 7 and 10 months.

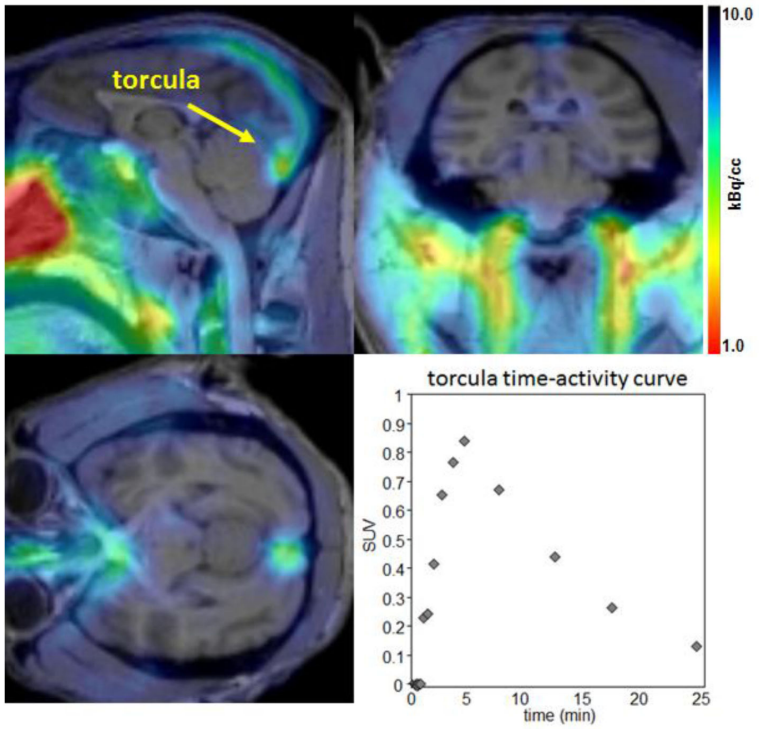

Figure 2.

Summed PET (0-15 min) with structural MR images (top). Radioactivity is seen primarily in the confluence of the sinuses (torcula) with the highest intensity just inside the occipital protuberance (lower left). Time-activity curve for the radioactivity observed is also shown (bottom right).

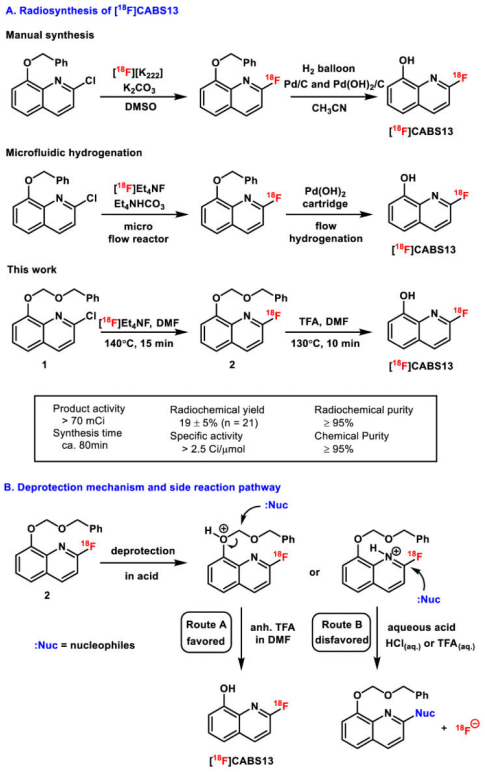

Scheme 1.

Improved radiosynthesis of [^{18}F]CABS13 based on benzyloxymethyl precursor 1. (A) Reaction conditions and radiosynthesis results. (B) Plausible mechanism of trifluoroacetic acid mediated deprotection and formation of side products under aqueous acidic conditions.